agriculture

MDPI

Article

Research on the Sugarcane Stubble Chopping Mechanism of an Ultra-Deep Vertical Rotary Tillage Cutter Based on FEM-SPH Coupling Method

Wang Yang, Huangsheng Lu, Xiong Xiao, Zhengkai Luo, Weilong Dai and Zhiheng Lu *

College of Mechanical Engineering, Guangxi University, Nanning 530004, China
* Correspondence: 8812316@163.com

Abstract: After existing ultra-deep vertical rotary tillers work in sugarcane stubble fields, the stubble chopping performance is poor, and the reason for this is unknown. To solve this, this paper develops a simulation model of ultra-deep vertical rotary tillage (UDVRT) in a sugarcane stubble field using the FEM-SPH coupling method and physical testing. The simulation model is used to investigate the rotary tillage process in the stubble field and the stubble chopping mechanism of the UDVRT cutter, identifying the causes of inadequate stubble chopping effectiveness. The results show that, when comparing the simulation with the field test, the magnitude and variation of the cutter's torque curves are relatively consistent, the relative error of the topsoil fragmentation rate is 9.5%, the entire cultivated layer of soil fragmentation rate is 11.3%, and the average number of times the stubble stem was cut off is closer; thus, the modeling method of the simulation model is reasonable and accurate. When the cutter cuts the soil and the stubble simultaneously, the soil's constraint on the stubble is gradually weakened, the velocity difference between the blade and the stem becomes smaller, the tilt of the stems becomes larger, and the number of times the blade can cut the stems reduces, leading to the poor chopping effect of stubble. The cutter cuts the stubble in the order of the blade from top to bottom, with the blade cutting the stem first and then the root, which is an effective measure to increase the stubble fragmentation rate. The findings of this paper can provide a reliable theoretical basis for the optimal design of a UDVRT cutter.

Keywords: ultra-deep vertical rotary tillage; stubble chopping; cutter; FEM-SPH coupling method; mechanism

Academic Editor: Valentin Vlăduț

Received: 9 December 2024
Revised: 24 January 2025
Accepted: 27 January 2025
Published: 2 February 2025

Citation: Yang, W.; Lu, H.; Xiao, X.; Luo, Z.; Dai, W.; Lu, Z. Research on the Sugarcane Stubble Chopping Mechanism of an Ultra-Deep Vertical Rotary Tillage Cutter Based on FEM-SPH Coupling Method. *Agriculture* **2025**, *15*, 329. https://doi.org/10.3390/agriculture15030329

1. Introduction

Ultra-deep vertical rotary tillage (UDVRT) is a new tillage method that has been developed in China in recent years. It uses pairs of counter-rotating cutters on an ultra-deep vertical rotary tiller to cut the soil transversely, subsequently breaking and lifting. The working depth of the UDVRT is up to 30–50 cm, it can break the plow pan, and loosen the entire cultivated layer of soil, thus effectively increasing the yield of dry land crops [1–3].

Sugarcane is a perennial stalk crop, and, before planting, it is necessary to remove the sugarcane stubble from the field. The sugarcane stubble consists of the stems and roots. At present, the removal of sugarcane stubble is mainly carried out by horizontal rotary tiller for multiple operations, which is inefficient. In contrast, the UDVRT method can break both sugarcane stubble and soil in a single pass, offering high efficiency. However, when an ultra-deep vertical rotary tiller works in a sugarcane stubble field, its cutter is poor at chopping sugarcane stubble, and the reason for this is not yet understood. Therefore, it is essential to conduct a study on the cutter's chopping sugarcane stubble mechanism and discover the

reasons for the poor chopping effect of the stubble. The study will provide a foundation for the optimization design of the UDVRT cutter used in the sugarcane stubble field.

In 2010, Wei Benhui and Li Shenwen et al. invented an ultra-deep vertical rotary tiller, which was initially towed by a tractor, and later developed a new type of self-propelled ultra-deep vertical rotary tiller [4,5]. However, both machines worked with significant resistance and operated with low efficiency. Additionally, the cutter is the key component of the ultra-deep vertical rotary tiller, meaning that its structure directly affects the tillage effect. When existing cutters work in the field, there are some issues, such as significant resistance, high vibration amplitude, and low topsoil fragmentation rate after tillage. Yang Wang's team addressed these issues by using the SPH method to establish a simulation model. This model was used to investigate how cutter structure parameters affect operational performance and soil fragmentation rate. Based on these findings, they designed new tillage components, resulting in improved working performance of machines in the field [6–11]. Wei Benhui invented a new cutter [12], which has two vertical cutter arms fixed on a circular cutter disc, and the blades are perpendicularly arranged on the surface of the arms. However, the cutter does not have a significant effect of resistance reduction in actual operation. The above literature shows that the research on ultra-deep vertical rotary tillers is still in its early stages, and there is limited research on the UDVRT cutter chopping sugarcane stubble in the field.

Since sugarcane stubble is buried within the soil, it is difficult to observe the process of the cutter breaking the stubble through physical tests, so as to find out the chopping stubble mechanism. However, simulation allows the process by which the cutter cuts the soil and stubble to be observed and it provides an effective way to study the interaction between the tillage components and the stubble–soil system. Therefore, simulation is a feasible method for investigating the mechanism of the UDVRT cutter chopping sugarcane stubble. The commonly used simulation methods are finite element method (FEM), discrete element method (DEM), and smooth particle hydrodynamics (SPH). FEM is a mesh-based numerical method that requires less time to solve problems. However, it is prone to mesh distortion during large deformations, leading to non-convergence issues. Using the FEM method, researchers have developed simulation models for blade–corn stubble–soil and blade–fruit tree root–soil interactions [13–15]. In contrast, DEM does not rely on mesh, making it effective for simulating soil fragmentation and large deformations, but its contact parameters are difficult to determine [16]. Using the DEM method, simulation models have been built for disc plow–soil–corn stubble, shovel–spinach root–soil, and chopping stubble blade–stubble–soil interactions [17–19]. The SPH method, a particle-based discretization method that does not require meshing, is well-suited for simulations with large deformations [20]. Furthermore, it uses the fundamental theory of continuum medium mechanics, which applies to the constitutive relations of various materials. Therefore, the SPH method is an effective method currently used to study soil–tillage component interactions and has been widely used to simulate large soil deformations [21–27]. However, in the simulation of the stubble–soil-tillage component system, the soil undergoes large deformations, while the stubble experiences relatively minor deformation. To more effectively simulate the large soil deformation, reduce computational time, and simplify the calibration of soil mechanical properties, it is more appropriate to adopt the coupled method of FEM-SPH.

Therefore, in order to determine the causes of the poor effect of the UDVRT cutter when chopping sugarcane stubble, the paper first uses the FEM-SPH coupling method to establish the simulation model of UDVRT in the sugarcane stubble field. The simulation model is then utilized to investigate the mechanism of cutter chopping sugarcane stubble and to analyze the causes of poor stubble-chopping performance. The results of the study will provide a theoretical basis for the structural optimization of cutters that are designed for sugarcane stubble chopping.

2. Materials and Methods

2.1. FEM-SPH Coupling Theory

In the coupling process of FEM-SPH re-calculation, within the approximate radius of the interface near SPH particles, different approximation methods are adopted according to different positions and discrete patterns [28]. For particles close to the coupling interface, the finite element nodes in the support domain are added to the summation in the form of background particles. When far away from the coupling boundary, SPH particles only adopt the SPH particle form, and the finite element only adopts the finite element form. The following are the three approximation formulas for SPH, FEM, and FEM-SPH respectively [29].

$$< f(x_i) >= \sum_{j=1}^{N} \frac{m_j}{\rho_j} f(x_{ij}) W_{ij}, \tag{1}$$

$$< f(x) >= \sum_{i} N_i(x) f(x_i), \tag{2}$$

$$< f(x_i) >= \sum_{j=1}^{N} \frac{m_j}{\rho_j} f(x_j) W_{ij} + \sum_{j=1}^{N_b} \frac{m_{bj}}{\rho_{bj}} f(x_j) W_{ij}. \tag{3}$$

Equation (1) is the SPH particle equation, Equation (2) is the finite element equation, and Equation (3) is the SPH-FEM coupling equation. In these equations, N_b represents the number of particles within the support domain, m_{bj} represents the mass of a particle, ρ_{bj} represents the density of a particle, and $N_i(x)$ represents the finite element shape function. Figure 1 shows the flow chart of the SPH-FEM coupling process.

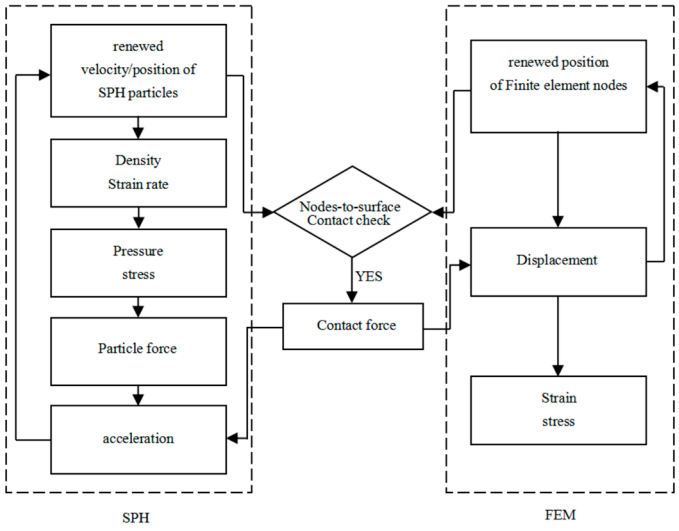

Figure 1. Flow chart of the SPH-FEM contact algorithm.

2.2. Structure and Working Principle of the Ultra-Deep Vertical Rotary Tiller

The ultra-deep vertical rotary tiller mainly consists of a chassis, cab, engine, hydraulic lifting device, and ultra-deep vertical rotary tillage device, as shown in Figure 2. The ultra-deep vertical rotary tillage device mainly includes a transmission box and tillage components. The tillage components are the key parts of the ultra-deep vertical rotary tiller, consisting of a row of cutters, with adjacent cutters rotating in opposite directions. Each cutter comprises a spiral blade, shaft, and blade, as shown in Figure 3. When the ultra-deep vertical rotary tiller is in operation, the cutter starts to rotate, and then the hydraulic lifting device is activated to lower the cutter to drill into the soil, reaching the required tillage depth. Finally, the rotating cutter moves forward with the machine, constantly cutting the soil and sugarcane stubble.

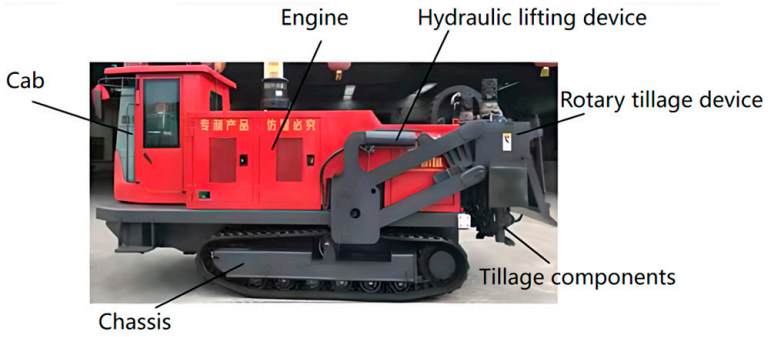

Figure 2. Ultra-deep vertical rotary tiller.

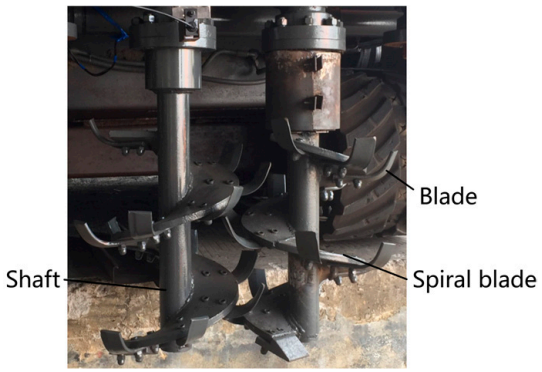

Figure 3. Cutter.

2.3. Ratoon Sugarcane Pull-Down Test

The test was conducted in December 2019, and the sugarcane variety was GT46. The test site was located in Quli Town, Fusui County, Chong Zuo, Guangxi, China (E107°45′11″, N22°31′33″). The soil at this site is sandy clay loam, with an average hardness and average moisture content of 10.35 kg·cm^{-2} and 16.33%, respectively. A second-year ratoon sugarcane—with good growth, featuring two stalks, and free from pests and diseases—was selected as the test sample. As per [16], the main test equipment was a self-made tension sensor, a dynamic tester (type: Donghua DH5981, Donghua Testing Technology Co. Ltd., Jingjiang, China), a computer, an NEC high-speed camera (HotShot e1024), a self-made force measuring frame, a mobile power supply, and a white curtain. The tension sensor consists of a thin rectangular steel plate and two sets of strain gauge which are pasted on the upper and lower surfaces of the thin steel plate, respectively. A set of the strain gauge have two pieces. The bridge connection of the strain gauge is a full bridge connection. The tension sensor is calibrated by static calibration method. The force measuring frame is composed of a fixed rod and a parallel frame, and the two are connected by hinges.

Before testing, sugarcane stalks were cut using a saw, leaving only the portion below 60 cm above the ground. The two stalks were then tied together, and the clamp was mounted to them at a height of 50 cm from the ground. Ropes are used to connect the two ends of the tension sensor to the parallel frame and the clamp, respectively, in order to measure the horizontal pulling force F when the sugarcane is tilted. Meanwhile, a tracking point was set 10 cm below the clamp, and the displacement of this tracking point was measured by the high-speed camera. Finally, through the relationship between the displacement and time, the curve of the sugarcane's inclination angle β was obtained. The diagram of the test system is shown in Figure 4, and the testing site is shown in Figure 5.

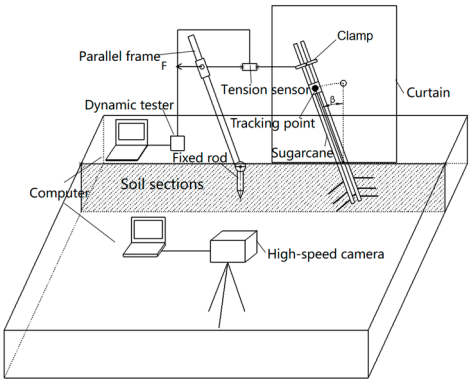

Figure 4. Diagram of the test system.

Figure 5. The site of the pull–down test for ratoon sugarcane.

2.4. Measurement of Soil and Sugarcane Parameters

To build the ratoon sugarcane pull-down simulation model, the parameters of soil and sugarcane samples in the pull-down test were measured. The soil was divided into five layers, each with a thickness of 10 cm, and the soil parameters for each layer were measured separately. Equipment for measuring soil parameters include a triaxial compression apparatus (type: TSZ-2, Ningxi Soil Instrument Co., Ltd., Nanjing, China). The elastic modulus, cohesion, internal friction angle, and Poisson's ratio of the soil were measured using the method of measurement found in [30]. The main soil property parameters of each layer are shown in Table 1. For measuring sugarcane parameters, the root–soil mixture was excavated carefully to avoid damaging the roots. The dimensions of the root–soil mixture were measured, and then the roots were cleaned of soil (as shown in Figure 6). The equipment for measuring sugarcane parameters are as follows: electronic scales (accuracy, 0.01 g), large measuring cylinders (accuracy, 5 mL), small measuring cylinders (accuracy, 1 mL), a universal testing machine (type: NKK-4005; maximum load, 5 KN; accuracy, 0.1 N; Nanfang Precision Instrument Co., Ltd., Shenzhen, China). The density, modulus of elasticity, Poisson's ratio and the yield stress of sugarcane were obtained as per [31]. The geometric parameters of sugarcane were measured by referring to the method in [16]. The root–soil mixture was approximately cylindrical, with a diameter of 373 mm and a height of 239 mm. The height of both stalks of the sample was 600 mm, and the heights of the left stem and the right stem were 181 mm and 152 mm, respectively. The average diameter of the left stalk and stem was 33.5 mm, while the average diameter of the right stalk and stem was 30.9 mm. The geometry parameters of the root system are shown in Table 2. The property parameters of the stalk and stem were averaged, and Table 3 shows the main property parameters. Table 4 shows the main property parameters of the roots.

Table 1. The main property parameters of the soil.

Soil Layer	Solid Parameters				
	Soil Density/kg·m^{-3}	Moisture Content/%	Cohesion/KPa	Internal Friction Angle/°	Elasticity Modulus/MPa
1	1661.45	13.22	14.764	26.89	3.0
2	1683.34	14.18	51.002	25.97	6.3
3	1710.29	17.00	84.950	25.59	8.2
4	1738.93	20.92	96.951	25.08	9.0
5	1725.45	20.56	95.814	25.36	8.8

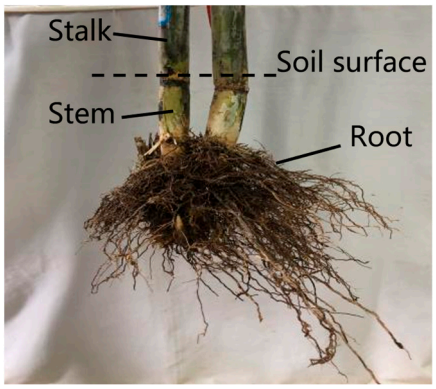

Figure 6. Ratoon sugarcane.

Table 2. The main geometric parameters of the root.

Layer	Number n/bar	Average Length L/mm	Average Diameter d/mm	Average Angle Between Root and Level Axis α/°	Depth h/mm
1	16	143.2	1.15	27.92	45
2	104	137.8	1.21	38.86	94
3	40	118.9	1.04	47.78	141

Table 3. The main property parameters of the stalk and stem.

Part	Average Density/kg·m^{-3}	Average Elasticity Modulus/MPa	Poisson Ratio	Average Yield Stress/MPa
Stalk	1075.50	63.48	0.32	-
Stem	955.74	57.25	0.30	2.9

Table 4. The main property parameters of the root.

Layer	Average Density/kg·m^{-3}	Average Elasticity Modulus/MPa	Equivalent Average Density/kg·m^{-3}	Equivalent Average Elasticity Modulus/MPa	Poisson Ratio	Average Yield Stress/MPa
1	682.91	527.45	45.24	34.94		
2	654.75	549.71	48.02	40.31	0.29	10.8
3	715.93	537.73	38.79	29.13		

2.5. Cutting Sugarcane Stubble Test

A well-grown ratoon sugarcane with two stalks, located 1 m away from the sugarcane sample used in the pull-down test, was selected. It and the sugarcane sample used in the pull-down test belong to the same plot, share the same variety and growing period,

and its stubble was dug out for use as the test sample. The main test equipment included the following: an electronic universal testing machine (type: NKK-4005; maximum load, 5 KN; accuracy, 0.1 N; Nanfang Precision Instrument Co., Ltd., Shenzhen, China), blade (same material as the blades of cutter), stem-cutting base (a three-point bending fixture), and a root-cutting base (with a slot in the center that is 2 mm wide and 50 mm long). The blade dimensions, along with the stem-cutting and root-cutting tests, are shown in Figures 7 and 8. The geometric parameters of the sugarcane stubble samples for the cutting test were measured using the measurement methods in Section 2.4. The diameters of the two stems of the stubble were 32 mm and 30 mm, with lengths of 170 mm and 155 mm, respectively. To ensure that the root-cutting test was representative, one root from each layer, close to the average diameter of the roots in that layer, was selected for testing. The lengths of the roots selected from the first to third layers were 132.2 mm, 126.8 mm, and 110.6 mm, and the diameters were 1.04 mm, 1.2 mm, and 1.02 mm, respectively.

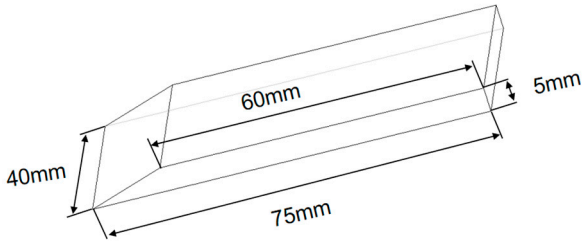

Figure 7. The blade sizes.

(**a**) (**b**)

Figure 8. Cutting sugarcane stubble test. (**a**) Stem-cutting test. (**b**) Root-cutting test.

Before conducting the stem-cutting test, the gauge length of the three-point bending fixture was set to 2 cm, and the downward cutting velocity of the blade was adjusted to 600 mm/min. The stem-cutting force curve was obtained through the test. The cutting force was averaged from the two stems after they were cut. For the root-cutting test, the roots were laid flat on the root-cutting base, with their ends secured using adhesive tape. The downward cutting velocity of the blade was set to 24 mm/min, and the root-cutting force curve was obtained through the test.

2.6. UDVRT Test in the Sugarcane Stubble Field

The ultra-deep vertical rotary tillage (UDVRT) test was conducted in January 2021, using the sugarcane variety GT46, which was the same as that used in the pull-down test. The testing site was located in Wuming District, Nanning City, Guangxi (E108°7′37″, N23°9′4″), where the soil is also sandy clay loam. The average hardness and moisture content were 9.8 kg·cm^{-2} and 15.1%, respectively, which were almost consistent with the soil in the pull-down test. The test equipment included the ultra-deep vertical rotary tiller, a self-made torque transducer, a DH5902 wireless torque test system, a laptop, and mobile power. The testing site is shown in Figure 9.

Figure 9. The test site of UDVRT.

We referred to [6] to conduct the test, with the tillage depth in the test set to 40 cm, the rotary velocity of the cutter 400 r/min, and the advance velocity of the cutter 0.5 m/s. The torque of the cutter was measured during the tillage process. According to [32], the soil fragmentation rate was measured. The average number of times the stem was cut off was measured. Because the field test could only count the number of fracture surfaces of the stem, this number was used as a proxy for the number of times the stem was cut off. The test was repeated three times, and the test results were averaged.

2.7. Modeling of Ratoon Sugarcane Pull-Down System

2.7.1. Geometrical Model

The geometric morphology of ratoon sugarcane is complex, and the sample of the pull-down test is shown in Figure 6. To facilitate the modeling and reduce computational time, the ratoon sugarcane model was simplified, following the approach in [16]. The geometric model is shown in Figure 10 where h_1, h_2 and h_3 represent the growth depths of the first to third layers of roots, respectively; α_1, α_2 and α_3 represent the growth angles of the first to third layers of roots, respectively; L_1, L_2 and L_3 represent the lengths of the first to third layers of roots, respectively, and H represents the length of the stem. Except that the circular cross-section of the roots is simplified to a rectangle with dimensions of 8 mm × 1 mm, the remaining dimensional parameters of the sugarcane model are consistent with those in Section 2.4 and Table 2. The geometry of the soil model was based on the size of the root–soil mixture, and, to reduce computation time, the geometric dimensions of the soil model were set to 1200 mm × 1000 mm × 430 mm (L × W × H).

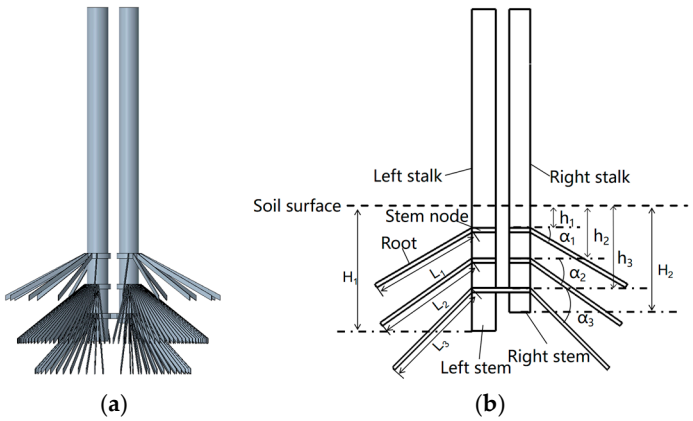

Figure 10. Geometric model of ratoon sugarcane. (**a**) Three-dimensional model. (**b**) Geometric dimension annotation.

2.7.2. Material Model

According to [16], the material model of sugarcane was MAT_ELASTIC, and the material model of soil was MAT_FHWA_SOIL. The material model parameters of stalk and stem are shown in Table 3. Because the stem node has a small influence in the simulation in this paper, its material model parameters were set to be consistent with the stem. Due to adjustments in the shape and size of the roots during modeling, their measured average density and average elastic modulus were equivalently transformed as per [16], while the rest of the material parameters remain unchanged, the material model parameters of the root are shown in Table 4, and, based on the main property parameters of the soil in Table 1, the parameters of the soil material model are shown in Table 5.

Table 5. The parameters of the soil material model.

Property	Value				
	Layer 1	**Layer 2**	**Layer 3**	**Layer 4**	**Layer 5**
Mass density, RO	1661.45	1683.34	1710.29	1738.93	1725.45
Plotting options, NPLOT	1	1	1	1	1
Specific gravity of soil, SPGRAV	2.79	2.79	2.79	2.79	2.79
Density of water in model units, RHOWAT	1000	1000	1000	1000	1000
Viscoplasticity parameter, VN	1.1	1.1	1.1	1.1	1.1
Viscoplasticity parameter, GAMMAR	0	0	0	0	0
Maximum number of plasticity iterations, INTRMX	10	10	10	10	10
Bulk modulus, K	2.5×10^6	5.25×10^6	6.833×10^6	7.5×10^6	7.33×10^6
Shear modulus, G	1.154×10^6	2.423×10^6	3.154×10^6	3.462×10^6	3.325×10^6
Peak shear strength angle, PHIMAX	0.4693	0.4533	0.4466	0.4377	0.4396
Coefficient A for modified Drucker–Prager surface, AHYP	1455.7000	5235.3999	8869.2002	1.036×10^4	1.018×10^4
Cohesion n shear strength at zero confinement, COH	1.476×10^4	5.1×10^4	8.495×10^4	9.695×10^4	9.347×10^4
Eccentricity parameter for third invariant effects, ECCEN	0.7	0.7	0.7	0.7	0.7
Strain hardening percent of PHIMAX where non-linear effects start, AN	0.2	0.2	0.2	0.2	0.2
Strain hardening amount of non-linear effects, ET	0.1	0.1	0.1	0.1	0.1
Moisture content of soil, MCONT	0.1322	0.1418	0.1700	0.2092	0.2056
Parameter for pore water effects on bulk modulus, PWD1	0	0	0	0	0
Skeleton bulk modulus–pore water parameter n, PWKSK	0	0	0	0	0
Parameter for pore water effects on the effective pressure, PWD2	0	0	0	0	0
The minimum internal friction angle, PHIRES	0	0	0	0	0
Volumetric strain at initial damage threshold, DINT	0.0025	0.0025	0.0025	0.0025	0.0025
Void formation energy, VDFM	0.005	0.005	0.005	0.005	0.005
Level of damage that will cause element deletion, DAMLEV	0.5	0.5	0.5	0.5	0.5
Maximum principle failure strain, EPSMAX	0.99	0.99	0.99	0.99	0.99

2.7.3. Meshing, Contact Definition, Boundary and Loading

Hypermesh software (https://altair.com/hypermesh) was used for mesh generation. The geometrical models of the stem, stalk, stem node, root, and soil were divided into hexahedral mesh using the solid map method. The mesh size of the stem, stalk, and stem node was 7 mm, and the mesh size for the soil and root was 8 mm. Ultimately, all the soil meshes were transformed into SPH particles, and the particle number was 1,157,388.

The contact between the left and right stalks was determined with "AUTOMATIC SURFACE TO SURFACE" [16]. The coupling between the SPH soil particles and the FEM stem, as well as the SPH soil particles and the FEM root, were defined by "TIED NODES TO SURFACE" contact. The static and dynamic friction factors between the roots and soil were 0.53 and 0.35, respectively, and those between the stem and soil were 0.51 and 0.44, respectively, the remaining contact parameters are defined according to the default values in the keyword manual of LS-dyna software (https://www.ansys.com/products/structures/ansys-ls-dyna).

The remaining surfaces of the soil were fully constrained, except for the top surface. Referring to [16], in the simulation model we applied the horizontal pulling force F measured

from the physical pull-down experiment for ratoon sugarcane to the points on the surface of the two sugarcane stalks, 50 cm above the ground. The tilt angle curve of sugarcane was obtained through the simulation test, and the simulation model is shown in Figure 11.

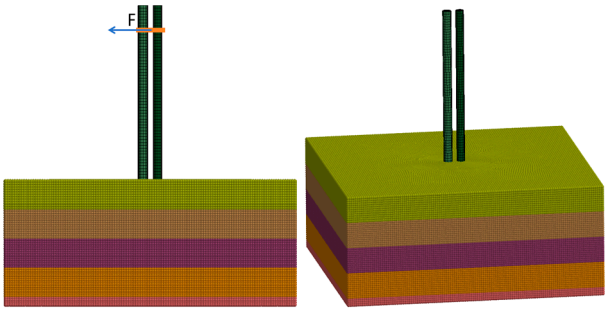

Figure 11. The simulation model of ratoon sugarcane pull-down. (**a**) Front view. (**b**) Axonometric view.

2.8. Modeling of Cutting Sugarcane Stubble

2.8.1. Geometric Model

The stem and root were simplified and modeled based on the method described in Section 2.7.1 and the dimensions provided in Section 2.5.

2.8.2. Material Model

Because the stem and root will be broken during the simulation, as noted in [16], their material model was defined as MAT_PLASTIC_KINEMATIC. The material model parameters of the stem and root are shown in Table 6. The material model for the blade, three-point bending fixture, and the root-cutting base was MAT_RIGID, with a density of 7800 kg/m^3, an elasticity modulus of 200 MPa, and a Poisson ratio of 0.27 [33].

Table 6. The material model parameters of the stem and root.

Property	Value			
	Stem	Root		
		Layer 1	Layer 2	Layer 3
Mass density, RO	955.74	45.24	48.02	38.79
Young's modulus, E	5.725×10^7	3.494×10^7	4.031×10^7	2.913×10^7
Poisson's ratio, PR	0.3	0.29	0.29	0.29
Yield stress, SIGY	2.9×10^6	1.08×10^7	1.08×10^7	1.08×10^7
Tangent modulus, ETAN	2.9×10^5	4.8×10^5	4.8×10^5	4.8×10^5
Hardening parameter, BETA	0	0	0	0
Strain rate parameter C, SRC	100	100	100	100
Strain rate parameter P, SRP	10	10	10	10
Failure strain for eroding elements, FS	0.2	0.2	0.2	0.2

2.8.3. Meshing, Contact Definition, Boundary and Loading

The blade, root-cutting base, and three-point bending fixture were divided into hexahedral meshes. The mesh size of the blade was 8.5 mm, and the root-cutting base and the three-point bending fixture were 5 mm. The mesh division methods and mesh sizes of the root and stem were the same as in Section 2.7.3.

The contact between the blade and stem, as well as the blade and root, were determined with "AUTOMATIC SURFACE TO SURFACE" [16]. The static and dynamic friction factors between the blade and stem were 0.55 and 0.48, respectively, while those between the blade and root were 0.52 and 0.34, respectively. The three-point bending fixture, the root-cutting base, and the ends of the root were fully constrained. The cutting velocity, consistent with the physical test, was applied to the blades in the stem-cutting simulation model and the

root-cutting simulation model. The cutting force curves of the stem and the root were obtained through the simulation test. The stem-cutting simulation model and root-cutting simulation model are shown in Figure 12.

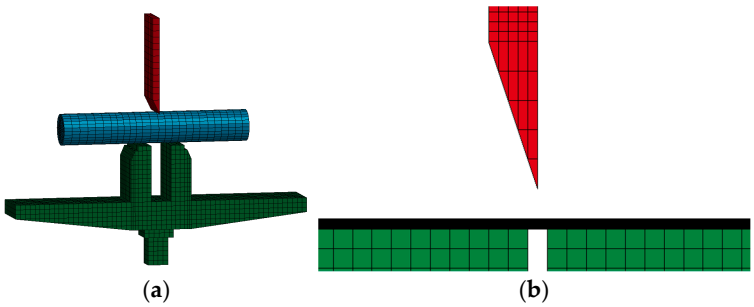

(**a**) (**b**)

Figure 12. Cutting sugarcane stubble simulation model. (**a**) Stem-cutting model. (**b**) Root-cutting model.

2.9. Modeling of UDVRT in the Sugarcane Stubble Field

The UDVRT in the sugarcane stubble field simulation model was constructed by integrating the modeling methods from the ratoon sugarcane pull-down simulation model and the cutting sugarcane stubble simulation model, along with the cutter cutting soil simulation model, as described in [6].

2.9.1. Geometric Model

The geometric model of the cutter was the same as that of the test prototype. The cutter consists of three parts: the shaft, the spiral blade and the blade, as shown in Figure 13. The shaft is 700 mm in height and 76 mm in diameter. The spiral blade has a pitch of 250 mm, a diameter of 300 mm and a thickness of 16 mm. The blade is shown in Figure 13b. For two adjacent blades on the cutter, the vertical distance between them is 40 mm, and the angle between them in the circumferential direction around the shaft is 60°. Due to the hilly and uneven terrain in most sugarcane-growing areas in China, harvesters find it difficult to harvest whole stalks. The average height of the residual stalks at the test site was measured at 4 cm. Therefore, the stalk of the sugarcane stubble model was set to a height of 4 cm, while the root and stem were the same as those of the geometrical model of the pull-down test. To meet the working width and depth requirements of the cutter, the soil sizes were consistent with those found in Section 2.7.1.

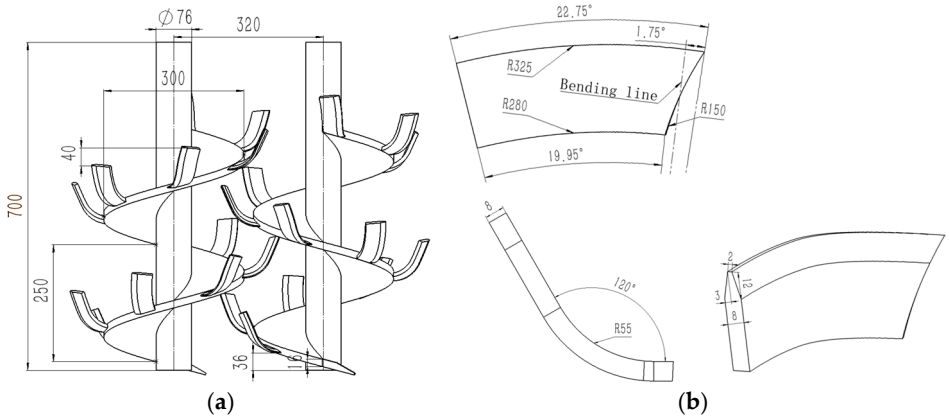

(**a**) (**b**)

Figure 13. Geometric model of the cutter. (**a**) Cutter. (**b**) Blade.

2.9.2. Material Model

In the simulation model, the stalk is considered a stem as it occupies only a small part of the sugarcane stubble model. The main property parameters and material model of

the stem and root were the same as those found in Section 2.8.2. Similarly, the property parameters and material model of the soil were the same as those found in Section 2.7.2. The cutters were made of the same material as the blades used in the cutting sugarcane stubble test, so their material model and property parameters were the same as for the blades in Section 2.8.2.

2.9.3. Meshing, Contact Definition, Boundary and Loading

The mesh of the blades on the cutter was divided in the same way and sizes as the blades in Section 2.8.3. The tetra mesh method was used to divide the shaft and spiral blades into tetrahedral meshes, with a mesh size of 7.5 mm. The soil and sugarcane mesh were divided in the same way and of the same sizes as in Section 2.7.3. According to [16,34], the contact between the cutter and the soil was determined with "AUTOMATIC NODES TO SURFACE," and the static and dynamic friction factors between them were 0.6 and 0.52, respectively. The contact setup between the cutter and stems, as well as the cutter and roots were the same as in Section 2.8.3, and the contact setup between the sugarcane and soil was the same as in Section 2.7.3. The rest of the soil surfaces were fully constrained, except for the top surface and the surface directly opposite the cutter. The forward and rotational velocities of the simulation model cutter were set to match those of the physical test. The simulation model of UDVRT in the sugarcane stubble field is shown in Figure 14.

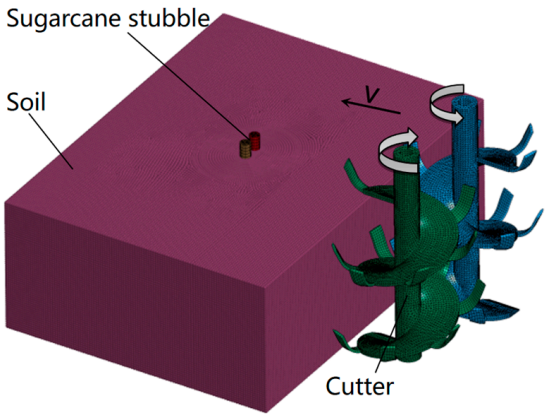

Figure 14. Simulation model of UDVRT in the sugarcane stubble field.

2.10. Model Verification

Because the sugarcane stubble is inside the soil, the cutter moves forward while rotating at high velocities. It is challenging for a single blade to sever the stem in one pass, thus direct validation of the sugarcane stubble–soil–cutter system models is difficult. Consequently, as referenced in [16], indirect methods are employed for validation. Firstly, referring to [16], the sugarcane stubble–soil system model is established and validated through a pull-down physical test. Then, the sugarcane stubble–cutter system model and the soil–cutter system model are built and validated through physical tests of the cutter cutting sugarcane stubble and cutting soil. Thereby, the rationality of the sugarcane stubble-soil-cutter system model can be verified indirectly. However, the validity of the soil-cutter system model has been verified in [6], and the cutter primarily relies on its blade to sever sugarcane stubble. Therefore, this paper focuses on validating the sugarcane stubble–soil and the sugarcane stubble–blade system model through the pull-down physical test and the blade cutting sugarcane stubble physical test, respectively [16]. Specifically, using the simulation of the ratoon sugarcane pull-down test and the cutting sugarcane stubble test, the tilt angle curve of sugarcane, and the stem and root cutting force curve were obtained. Then, those curves were compared with the corresponding physical test results to validate

the rationality of the sugarcane stubble–soil system and the sugarcane stubble–cutter system modeling method. Meanwhile, we conducted the UDVRT test in the sugarcane stubble field and then measured the cutter's torque, the soil fragmentation rate, and the breaking situation of stubbles. These metrics are used to validate the sugarcane stubble–soil–cutter system further. Specifically, through the simulation of the UDVRT test in the sugarcane stubble field, the cutter's torque variation curve, soil fragmentation rate, and the number of times the stem was cut off were obtained. Finally, the test results of simulation and physics were compared to further verify the validity of the simulation model of UDVRT in the sugarcane stubble field.

2.11. Methods for Analyzing the Sugarcane Stubble Movement and Cutting Sugarcane Stubble Velocity Difference Change

When the cutter works in the sugarcane stubble field, the ability to chop the stems depends on the blade's horizontal velocity relative to the stems (called the velocity difference). With a fixed-blade rotational velocity, a greater soil constraint on the sugarcane stubble results in less movement of the stubble, leading to a larger velocity difference and easier chopping of the stems. Therefore, this paper analyzes the soil's constraint on sugarcane stubble at different moments, the horizontal movement velocities of each area of the left and right stems during tillage, and the changes in velocity difference between the blade and the stem.

To facilitate analysis, this paper designates names for each part of the simulation model. After hiding the soil of the simulation model, as shown in Figure 15, the green cutter is called the left cutter, and the blue cutter is called the right cutter. Each cutter has 13 blades, with the blades of the left cutter numbered from 1L to 13L, in order from top to bottom, and the blades of the right cutter numbered from 1R to 13R. Along the direction of cutter advancement, the stem directly opposite the left cutter is called the left stem (the left stem together with its root is called the left half sugarcane stubble). The stem directly opposite the right cutter is called the right stem (the right stem together with its root is called the right half sugarcane stubble). The left stem was divided into 8 areas, and the right stem was divided into 7 areas, as shown in Figure 16.

When analyzing the soil's constraint on sugarcane stubble, the left and right halves of the sugarcane stubble are analyzed separately because of their different movements. To analyze the constraint, it is necessary to observe the contact between the sugarcane stubble and the surrounding soil. For clear observation, the model displays only the soil (the soil is cylindrical, with a diameter of 380 mm) around the sugarcane stubble and is viewed through a cross-section parallel to the cutter's forward movement direction and passing through the stem's central axis. The sugarcane stubble movement can be analyzed by the horizontal velocity curve of the stem, and the velocity difference change can be obtained based on the horizontal velocity curve of both the blade and the stem.

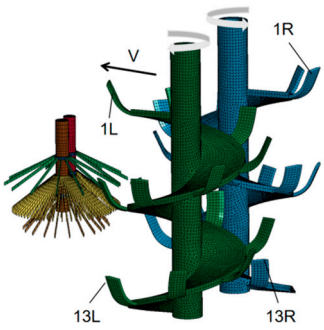

Figure 15. Schematic diagram of blade naming.

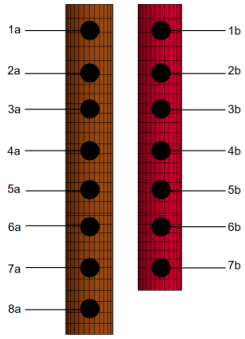

Figure 16. Name of each area of the two stems.

2.12. Methods of Analyzing the Chopping Process of Sugarcane Stubble

The chopping process of sugarcane stubble between the right half and left half is different. Therefore, to facilitate the analysis of the chopping process of sugarcane stubble, we divided this process into two parts: the first part describes the chopping process of the left half sugarcane stubble, and the second part describes the chopping process of the right half sugarcane stubble. Finally, we compare the two chopping stubble processes and count the number of times each blade on the left and right cutters cut the stem.

To clearly observe the entire chopping process, the soil is hidden. During the analysis chopping process of the left half sugarcane stubble, only the left cutter and the left half of the stubble are displayed. Conversely, when analyzing the chopping process of the right half sugarcane stubble, only the right cutter, the right half sugarcane stubble, and the 6L blades of the left cutter are displayed.

2.13. Methods of Analyzing Forces on Cutters During Tillage

When working in the sugarcane stubble field, the cutter simultaneously cuts the sugarcane stubble and the soil, encountering varying resistance from each. Different parts of the cutter experience different resistance when the cutter cuts the soil and the sugarcane stubble. Therefore, we divide the cutter into three parts—the blade, the shaft, and the spiral blade—and analyze their resistance while cutting through the sugarcane stubble and soil.

3. Results and Discussion

3.1. Model Verification

3.1.1. Sugarcane Stubble–Soil System Model Validation

Figure 17 shows the pulling force curve of the ratoon sugarcane pull-down physical test. Figure 18 shows the tilt angle curve of the ratoon sugarcane pull-down test, the black line is the physical test curve, and the red line is the simulation test curve.

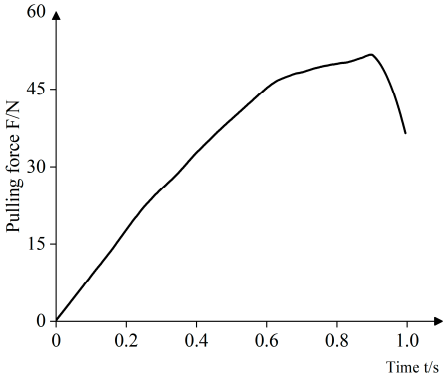

Figure 17. Pulling force curve.

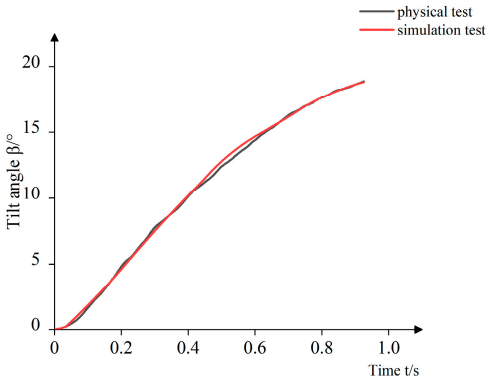

Figure 18. Tilt angle–time curve.

In Figure 18, the two curves follow the same trend, with the maximum relative error of 4.2%. The physical and the simulation test curves are relatively consistent, which indicates that the modeling method of the sugarcane stubble–soil system model is reasonable.

3.1.2. Sugarcane Stubble–Blade System Model Validation

Figure 19a shows the cutting force curves of the stem, and Figure 19b–d show the cutting force curves for the first second, and third layer of roots, respectively. In these figures, the black line is the physical test curve, and the red line is the simulation test curve.

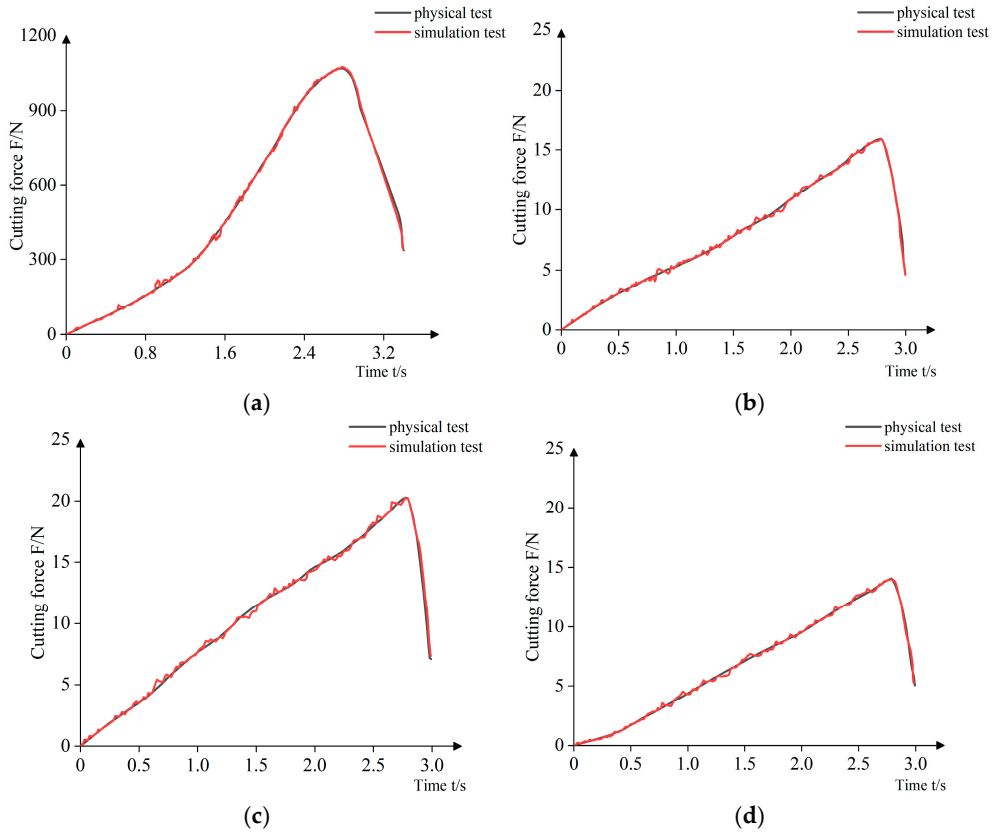

Figure 19. Cutting force of sugarcane stubble. (**a**) Cutting stem. (**b**) Cutting the first layer of the root. (**c**) Cutting the second layer of the root. (**d**) Cutting the third layer of the root.

Figure 19 shows that, in the comparison of the simulation with the field test, their curves follow the same trend, with the cutting force maximum relative error when cutting the stem being 4.59%, when cutting the first layer of the root being 4.44%, when cutting the second layer of the root being 6.73%, and when cutting the third layer of the root being

5.36%. The close consistency between the physical and simulation test curves indicates that the modeling method for the sugarcane stubble–blade system model is reasonable.

3.1.3. Sugarcane Stubble–Soil–Cutter System Model Validation

Figure 20 shows the cutter's torque variation curve, and Table 7 shows the soil fragmentation rate and the average number of times the stem was cut off. In Figure 20, the black line is the physical test curve, and the red line is the simulation test curve.

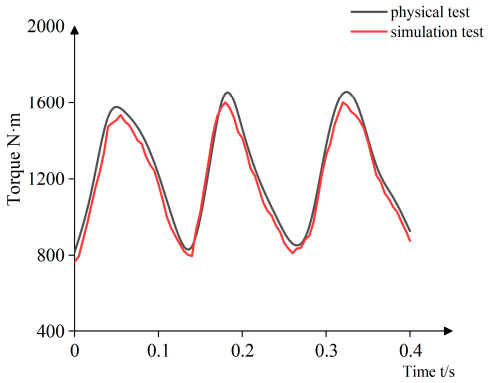

Figure 20. Torque curves.

Table 7. Soil fragmentation rate and the average number of times the stem was cut off.

Test Type	Topsoil/%	Full Soil/%	The Average Number of Times
Physical test	76.5	93.4	1.7
Simulation test	69.2	82.1	3.0

From Figure 20 and Table 7, we can see that the magnitude and variation of the torque curves from both the physical and simulation tests are relatively consistent, and that the torque maximum relative error is 5.98%. The relative error in the topsoil fragmentation rate is 9.5%, and in the entire cultivated layer of soil fragmentation rate, it is 11.3%. Furthermore, the average number of times the stem was cut off is closer, and the results of the simulation and physical tests are similar. These results suggest that the modeling method is reasonable, and that the simulation model of UDVRT in the sugarcane stubble field is applicable for analyzing the tillage process.

3.2. The Analysis of the Sugarcane Stubble Movement and Cutting Sugarcane Stubble Velocity Difference Change

Figure 21 is a sectional screenshot of the soil and sugarcane stubble as the cutter cuts the soil and stubble, with V representing the direction of the cutter's advancement. Figure 22 is a horizontal velocity diagram for each area of the sugarcane stubble stem. Figure 23 is a diagram of the horizontal cutting velocity at each point on the blade.

As can be seen in Figure 21, the soil is rapidly cut by the cutter, breaking into blocks of varying sizes that move upward and around, and the soil around the stubble loosens and swells. Thus, the soil's constraint on the stubble gradually weakens, and then the stubble tilts and moves with the soil. The process is similar to the results found [35].

As shown in Figures 21 and 22, when the cutter moves forward while cutting the soil and sugarcane stubble, the soil's constraint on the sugarcane stubble changes from strong to weak due to the disturbance caused by the cutter. During this phase, the stubble moves upwards and horizontally, driven by the cutter, and its horizontal velocity gradually increases. When most of the soil around the sugarcane stubble is cut, the soil's constraint on the stubble decreases sharply, meaning that it is not possible to cut the stubble. Due

to the lack of soil constraint, the stubble is propelled backward by the cutter, reaching its maximum horizontal velocity. Subsequently, as the cutter progresses, the stubble's velocity begins to decrease.

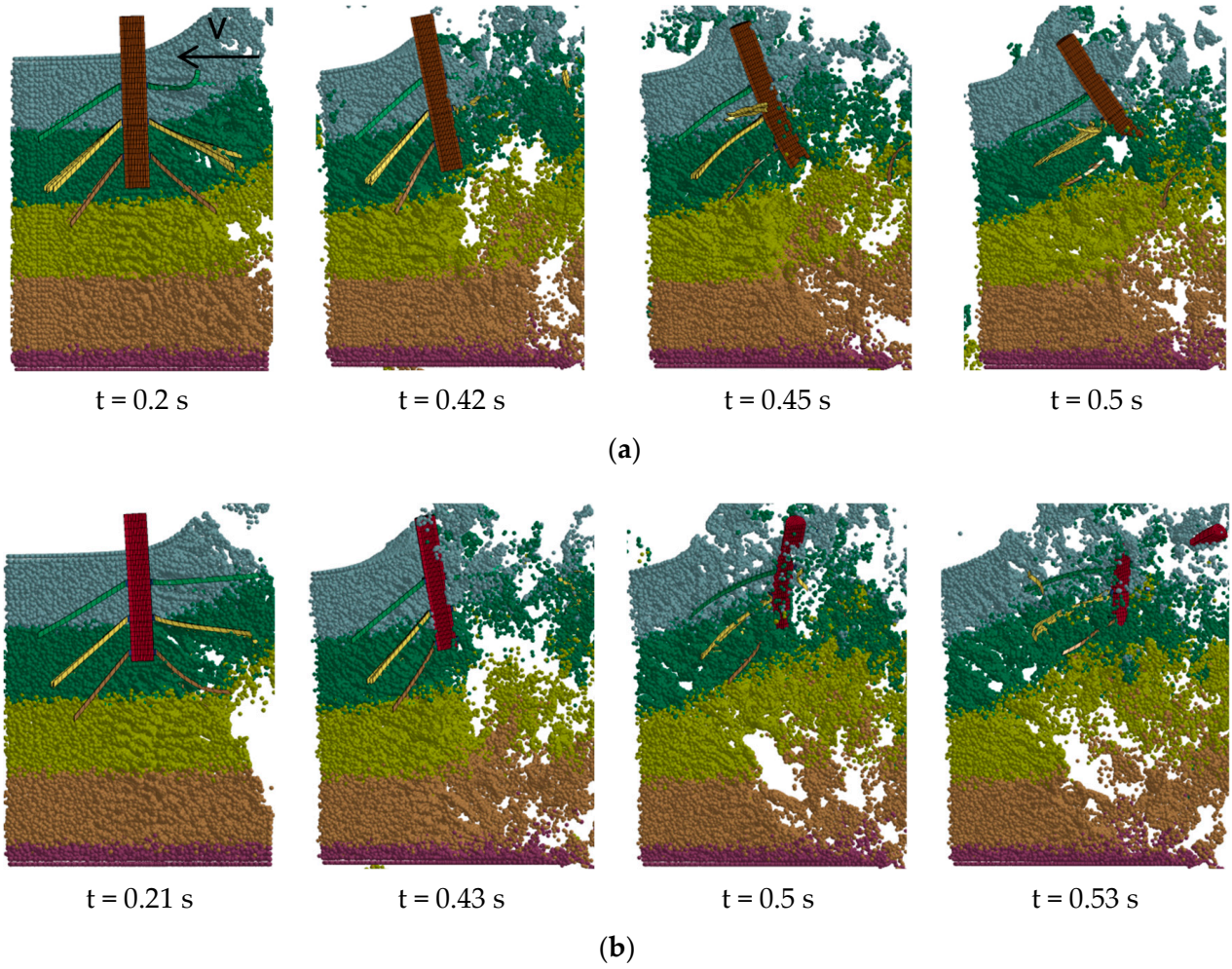

Figure 21. Diagram of changes in soil constraints on sugarcane stubble. (**a**) Left half sugarcane stubble. (**b**) Right half sugarcane stubble.

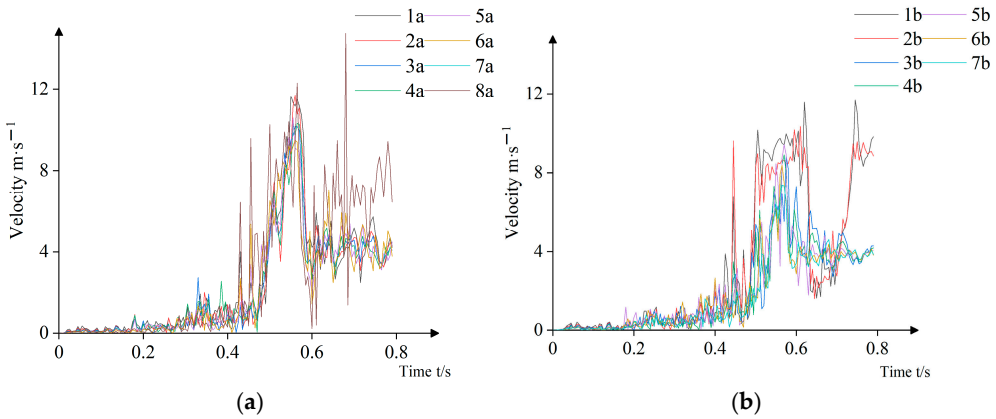

Figure 22. Horizontal velocity diagram for each area of the stem. (**a**) Left stem. (**b**) Right stem.

As can be seen from Figures 21–23, the soil's constraint on the sugarcane stubble progressively weakens as the cutter cuts the soil, and when the cutter advances and cuts the sugarcane stubble, the velocity difference between the stubble stem and blade gradually

decreases, making it increasingly challenging for the blade to chop the stem; if the velocity difference falls below a certain threshold, the blade will not effectively chop the stem. This shows that the soil's constraint on the sugarcane stubble is gradually weakened as the cutter cuts the soil and sugarcane stubble, from a strong constraint to a weak constraint. Consequently, the velocity difference when the blade cuts the stem decreases, which is a key factor contributing to insufficient chopping of the stem. To address this, the cutter structure should be optimized, so that when the blade cuts the stem, the soil can maintain a significant constraint on the stubble. This will enhance the velocity difference at the point of cutting, ensuring more effective chopping of the stubble.

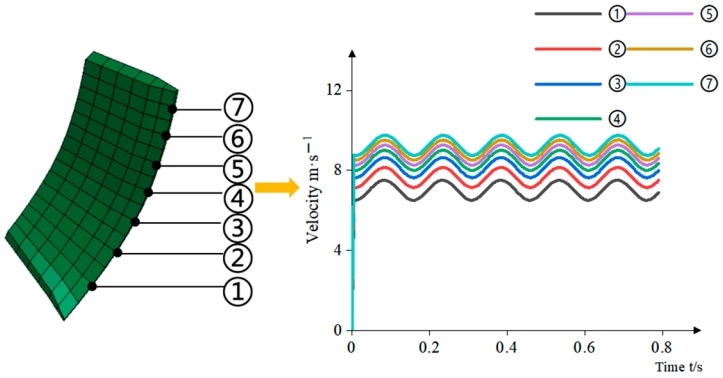

Figure 23. Horizontal cutting velocity at each point on the blade.

3.3. The Analysis of the Chopping Sugarcane Stubble Process

Figure 24 shows the process of the cutter chopping the left half of the sugarcane stubble.

When t = 0.42 s, the front half root of the left half sugarcane stubble has been cut off by the blade, and the stem is slightly tilted. When t = 0.425 s, point 7 on the 9L blade is about to cut at 8a of the stem, with a horizontal velocity difference of 7.83 $m \cdot s^{-1}$ between the blade and the stem. At t = 0.44 s, the 9L blade has not only chopped the stem at 8a but also bent the stem and cracked it at 6a. At this moment, the rear half root of the sugarcane stubble has not yet begun to be cut, and the magnitude of the stem tilt does not change much compared with 0.42 s. When t = 0.45 s, point 7 of the 8L blade is about to cut at 7a of the stem, with a horizontal velocity difference of 7.56 $m \cdot s^{-1}$ between the blade and the stem. By t = 0.465 s, the 8L blade chopped the stem at 7a, the fracture at 6a became larger, and the 8L blade also cut off the roots in the rear half of the third layer. At this time, the inclination of the stem significantly increased compared with at 0.44 s, due to the chopping of some roots in the rear half of the sugarcane stubble. When t = 0.48 s, the roots in the second layer are about to be cut off by the 7L blade. At t = 0.49 s, the root of the rear part of the sugarcane stubble was almost severed, and the inclination of the stem greatly increased. Additionally, point 7 of the 7L blade is about to be cut at 7a of the stem, with a horizontal velocity difference of 3.99 $m \cdot s^{-1}$ between the blade and the stem. At t = 0.5 s, the 7L blade cut through the stem, completely separating the fracture at 6a. However, at point 7a, only the surface of the stem node is scratched, and the stem cannot be further chopped due to the reduced velocity difference. When t = 0.53 s, the cutter can no longer cut the left half of the sugarcane stubble, marking the end of the cutting process. This process shows that the cutting effectiveness of the cutter on the left half of sugarcane stubble is limited. The primary reason is that, as the rear half of the roots are chopped, the soil's constraint on the stubble weakens, leading to a smaller velocity difference and greater stem inclination, which results in fewer effective cuts by the blades.

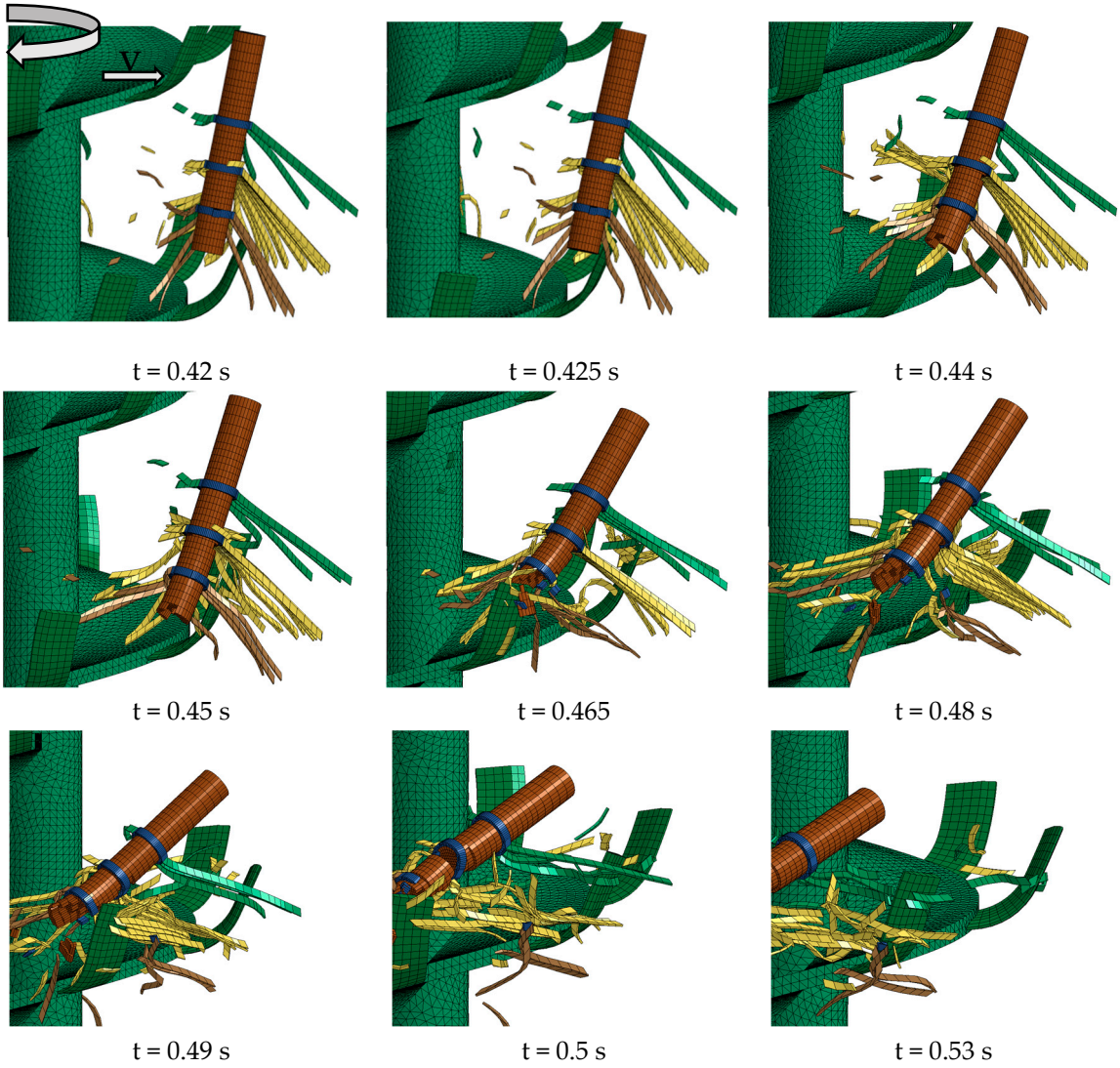

Figure 24. The cutting process of the left half sugarcane stubble.

Figure 25 shows the process of the cutter chopping the right half of sugarcane stubble.

As shown in Figure 25, when t = 0.415 s, the front half root of the right half sugarcane stubble is nearly severed, causing the stem to appear slightly tilted. Additionally, point 7 of the 6R blade is about to cut into 3b of the stem, with a horizontal velocity difference of 9.1 $m \cdot s^{-1}$ between the blade and the stem. When t = 0.43 s, the 6R blade has chopped the surface of the stem at 3b, and the tilting amplitude of the stem has little change compared with 0.415 s. At t = 0.44 s, point 7 of the 5R blade is about to cut into 3b of the stem, with a horizontal velocity difference of 7.3 $m \cdot s^{-1}$ between the blade and the stem. By t = 0.455 s, the 5R blade has chopped the stem's surface layer at the stem node, and all of the front half roots of the stem have been severed. The stem's tilt amplitude does not change much. When t = 0.485 s, point 4 of the 3R blade is about to cut at 2b of the stem, with a velocity difference of 6.3 $m \cdot s^{-1}$ between the blade and 2b of the stem. At t = 0.505 s, the 3R blade has cut the stem off and point 7 of the 6L blade of the left cutter is about to cut into the 5b of the stem with a velocity difference of 6.9 $m \cdot s^{-1}$ between the blade and the stem, while the stem is still only tilted slightly. When t = 0.52 s, the 6L blade has chopped the 5b of the stem, but the stem is not completely severed. At this time, point 1 of the 2R blade is about to cut the 3b of the stem, the horizontal velocity difference between the blade and the stem is 6.17 $m \cdot s^{-1}$, and the stem tilt amplitude does not change much. When t = 0.535 s,

the 2R blade has not only chopped the 3b of the stem, but the 5b has also been completely disconnected by the blade impact. At t = 0.56 s, the right half of the sugarcane stubble can no longer be cut by the cutter, and the cutting process is over. This process shows that the right half of sugarcane stubble is chopped more effectively. The reasons for this are that the rear half roots have not been chopped during the cutting process, resulting in greater soil constraint on the sugarcane stubble, a larger velocity difference, a smaller stem tilt, and more frequent cuts by the blades.

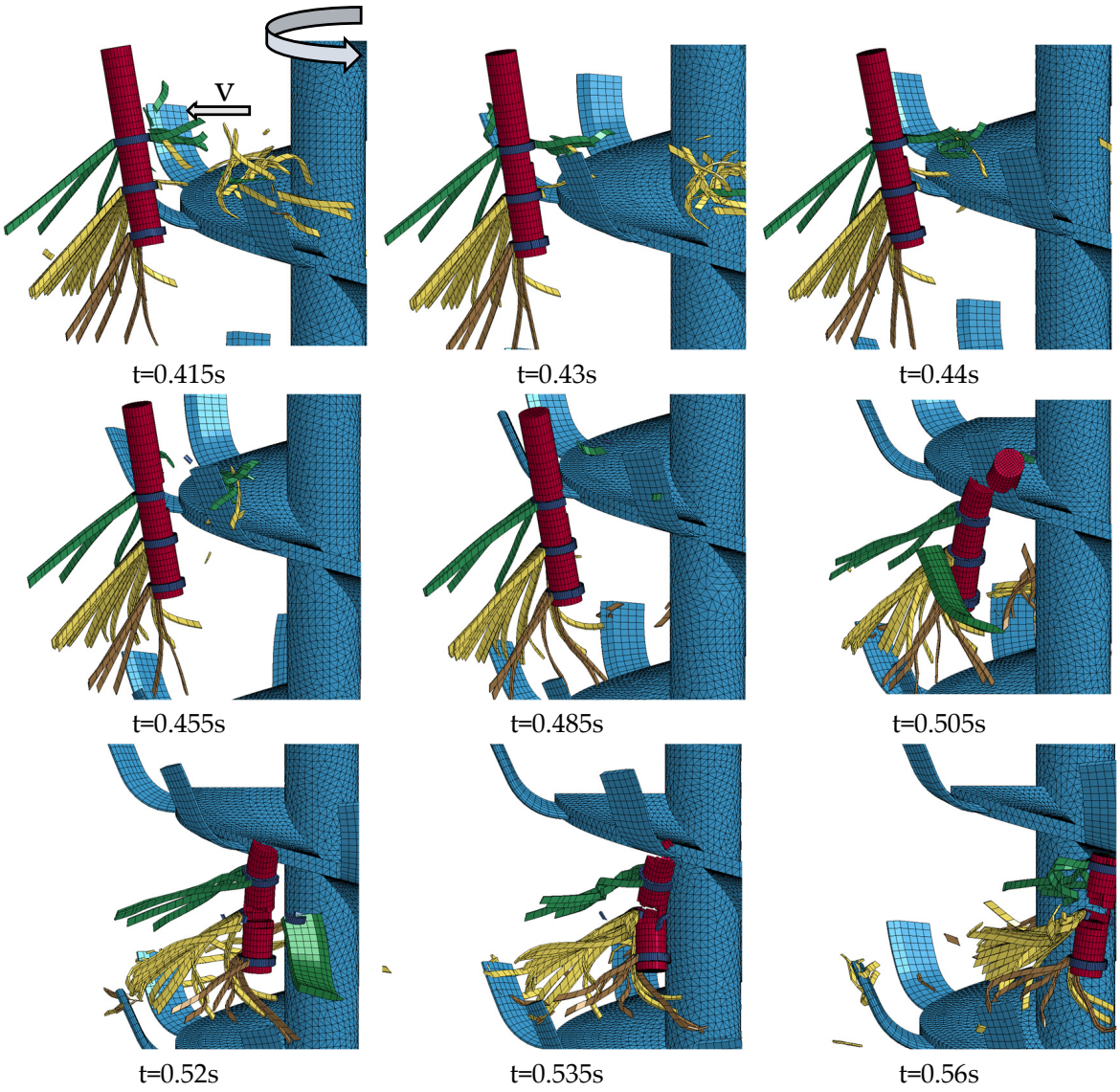

Figure 25. The cutting process of the right half sugarcane stubble.

Comparing the chopping process of the left and right half sugarcane stubble reveals key differences. The right half sugarcane stubble is cut from the top to the bottom, while the left half is cut from the bottom end to the top. When the cutter cuts from the bottom up, the roots are severed first, thus rapidly reducing the soil's constraint on the sugarcane stubble. As a result, by the time the blade cuts the stem, the velocity difference has significantly diminished, making it difficult for the blade to effectively chop the stem. In contrast, when the cutter cuts from top to bottom on the right half of sugarcane stubble, the rear half roots remain intact until the final stages of the cutting process. Thus, the soil can maintain significant constraints on the stubble, keeping a higher velocity difference as the blade cuts the stem. Consequently, the blade is better able to chop the stem efficiently.

During the entire chopping process of the sugarcane stubble, the blades 6L, 7L, 8L, and 9L of the left cutter and blades 2R, 3R, 5R, and 6R of the right cutter each cut the sugarcane stem once. It can be seen from this that the blades located at the bottom of the cutter failed to cut the stem, and that the blades that successfully cut the stem were concentrated in the middle and upper positions of the cutter. Among these, the blades in the middle region were the most frequently engaged. The reasons can be attributed to two key factors. First, the growth range of sugarcane stubble lies within the middle and upper positions of the cutter, so that the bottom blades are unable to reach and cut it. Second, during the cutting process, the sugarcane stem may tilt significantly, making it difficult for the top blades to reach the stem.

To improve the fragmentation rate of sugarcane stubble, the cutter structure should first be modified to enable a top-to-bottom cutting stubble sequence. Additionally, the arrangement and structure of the blades in the middle and upper positions of the cutter should be optimized to increase their frequency and effectiveness in cutting the stems.

3.4. The Analysis of Force on Cutter During Tillage

Figure 26 shows the resistance curves of the two cutters during the simulation test of the UDVRT in the sugarcane stubble field. Specifically, Figure 26a is the resistance experienced by the cutter from both the soil and sugarcane stubble. Figure 26b is the resistance experienced by different parts of the cutter when cutting the soil, and Figure 26c shows the resistance experienced by various cutter components when cutting the sugarcane stubble.

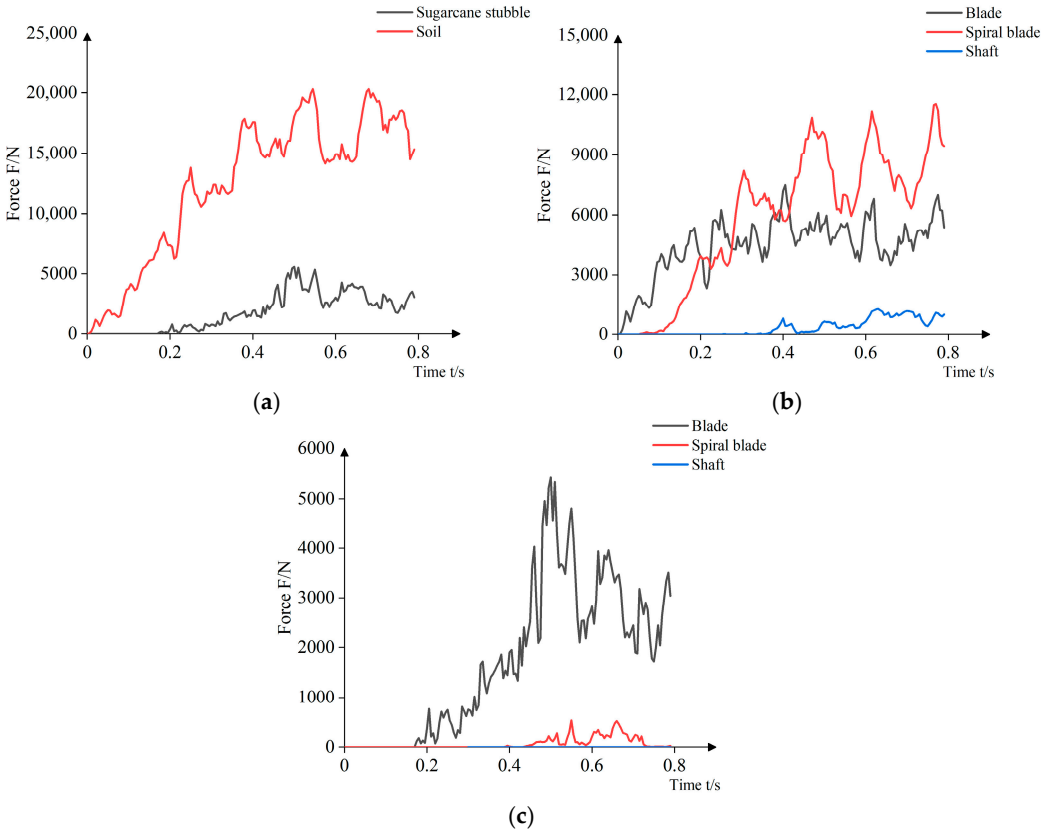

Figure 26. Resistance of cutter. (**a**) Cutter resistance to cutting soil and sugarcane stubble. (**b**) Resistance of each part of the cutter when cutting soil. (**c**) Resistance of each part of the cutter when cutting sugarcane stubble.

From Figure 26 it can be seen that, during the UDVRT in the sugarcane stubble field, the resistance of the cutter comes mainly from cutting the soil, with resistance from the

sugarcane stubble being relatively minor. During the stabilization phase (0.5–0.7 s), the average resistance of the cutter while cutting the soil was 15,880.4 N. Notably, 83.8% of this resistance was attributed to the blade and the spiral blades, while the shaft accounted for only 16.2%. In [6,8], when the same cutter was used for tilling an ordinary cultivated field, the proportions of the cutting soil resistance of the blade and the spiral blade were 88.5% and 86.6%, respectively, while those of the shaft were 11.5% and 13.4%, respectively. It can be seen from this that the analysis results of the cutter cutting soil resistance in this paper are similar to those in [6,8]. Therefore, the optimal design of blades and spiral blades for resistance reduction is required whether tilling in an ordinary cultivated field or in a sugarcane stubble field. When the cutter cuts the sugarcane stubble, the blade experiences the greatest resistance, while the spiral blades encounter little resistance, and the shaft is not subjected to any resistance.

4. Conclusions

This paper adopted the FEM-SPH coupling method to establish a simulation model of UDVRT in a sugarcane stubble field, researched the mechanism of a cutter chopping sugarcane stubble, explored the reasons for the poor chopping stubble performance, and analyzed the forces on the cutter during tillage. The main conclusions obtained are as follows:

(1) When the ultra-deep vertical rotary tiller works in the sugarcane stubble field, as the cutter cuts the soil around the sugarcane stubble, the soil's constraint on the stubble gradually weakens. Furthermore, the stubble tilts and moves with the soil. And when the cutter blade contacts the stubble, the stubble is cut. When the velocity difference between the blade and the stem reaches a certain value, the stem is cut off.

(2) When the cutter cuts the soil and the stubble simultaneously, the soil's constraint on the stubble is gradually weakened, the velocity difference between the blade and the stem becomes smaller, the tilt of the stems becomes larger, and the number of times the blade can cut the stems reduces, each of which are the main reasons for poor chopping performance on stubble. The cutter cuts the stubble in the order of the blade from top to bottom, the blade will cut the stem first and then the root, which is an effective measure to increase the stubble fragmentation rate.

(3) During tillage, the cutter primarily encounters resistance from its cutting into the soil. The average resistance experienced by the cutter when cutting the soil was 15,880.4 N, with 83.8% of this resistance acting on the blade and spiral blade, while only 16.2% was attributed to the shaft.

(4) It is suggested that an innovative structural design of the cutter be carried out to improve stem fragmentation and to reduce the resistance of the cutter when cutting the soil.

Author Contributions: Conceptualization, W.Y.; methodology, W.Y. and X.X.; software, H.L. and W.D.; validation, H.L. and Z.L. (Zhengkai Luo); writing—original draft preparation, H.L.; writing—review and editing, Z.L. (Zhiheng Lu) and W.Y.; project administration, W.Y. All authors have read and agreed to the published version of the manuscript.

Funding: This work was supported by grants from three foundations: 1. National Natural Science Foundation of China (grant number: 32160422); 2. National Natural Science Foundation of China (grant number: 51565003); 3. Guangxi Natural Science Foundation (grant number: 2023GXNSFAA026376).

Institutional Review Board Statement: Not applicable.

Informed Consent Statement: Not applicable.

Data Availability Statement: The data that support the findings of this study are available from the corresponding author upon reasonable request.

Conflicts of Interest: The authors declare no conflicts of interest.

References

1. Yin, J.; Zhang, X.; Ma, Y.; Yu, X.; Hou, H.; Wang, H.; Fang, Y. Vertical rotary sub-soiling under ridge–furrow with plastic mulching system increased crops yield by efficient use of deep soil moisture and rainfall. *Agric. Water Manag.* **2022**, *271*, 107767. [CrossRef]
2. Yao, R.; Gao, Q.; Liu, Y.; Li, H.; Yang, J.; Bai, Y.; Zhu, H.; Wang, X.; Xie, W.; Zhang, X. Deep vertical rotary tillage mitigates salinization hazards and shifts microbial community structure in salt-affected anthropogenic-alluvial soil. *Soil Tillage Res.* **2023**, *227*, 105627. [CrossRef]
3. Zhang, X.; Guo, J.; Ma, Y.; Yu, X.; Hou, H.; Wang, H.; Fang, Y.; Tang, Y. Effects of vertical rotary subsoiling with plastic mulching on soil water availability and potato yield on a semiarid Loess plateau, China. *Soil Tillage Res.* **2020**, *199*, 104591. [CrossRef]
4. Wei, B.; Li, S.; Gan, X.; Wei, Y.; Li, L. Rotary Cutting Type Deep Tillage Powder Ridge Multifunctional Machine. China Patent 201010270614.3, 26 December 2012.
5. Li, S. A Powder Ridge Machine for Sowing and Its Sowing Method. China Patent 201510285383.6, 21 September 2016.
6. Yang, W.; Xiao, X.; Pan, R.; Guo, S.; Yang, J. Numerical Simulation of Spiral Cutter–Soil Interaction in Deep Vertical Rotary Tillage. *Agriculture* **2023**, *13*, 1850. [CrossRef]
7. Yang, W.; Huang, Q.; Li, Y.; Han, Y.; Li, G.; Tang, Q.; Yang, J. Effect of Operating Performance of Deep Vertical Rotary Tillage Tool Based on SPH. *J. Agric. Mech. Res.* **2020**, *42*, 147–152.
8. Xiao, X.; Guo, S.; Zheng, X.; Pan, R.; Yang, J.; Yang, W. Simulation Study on Vibration Reduction of Powder Ridge Cutting Tool. *J. Agric. Mech. Res.* **2021**, *43*, 26–30.
9. Xiao, X.; Pan, R.; Zheng, X.; Yang, W. Simulation of Spiral Cutters Based on Soil Fragmentation Distribution. *J. Agric. Mech. Res.* **2021**, *43*, 29–34.
10. Sun, J.; Jiang, H.; Zheng, X.; Nong, H.; Zeng, B.; Yang, W. Simulation of Ultra Deep Rotary Tillage Tool Based on Soil Disturbance. *J. Agric. Mech. Res.* **2024**, *46*, 66–71.
11. Jiang, H.; Sun, J.; Zheng, X.; Huang, Y.; Yang, W. Research on Simulation Design of a New Type of Leafless Powder Ridge Cutter. *J. Agric. Mech. Res.* **2024**, *46*, 132–137.
12. Wei, B.; Zhang, X.; Wei, Y.; Ning, X. A Kind of Open Type Two Knives Drilling Powder Ridge Cutter. China Patent 202121165377.4, 3 May 2022.
13. Li, M.; Xu, S.; Yang, Y.; Guo, L.; Tong, J. A 3D simulation model of corn stubble cutting using finite element method. *Soil Tillage Res.* **2017**, *166*, 43–51. [CrossRef]
14. Mao, L.; Wang, P.; Yang, X.; Li, J.; Li, X.; Li, X. Design and Analysis of Vibratory Root System Cutting Device for Fruit Trees. *Trans. Chin. Soc. Agric. Mach.* **2020**, *51*, 281–291.
15. Shen, S. Shear Failure Characteristics of Root Soil Aggregates and Development of Bionic Desotption Cutter. Master's Thesis, University of Science and Technology Liaoning, Anshan, China, 2022.
16. Yang, W.; Zhao, W.; Liu, Y.; Chen, Y.; Yang, J. Simulation of forces acting on the cutter blade surfaces and root system of sugarcane using FEM and SPH coupled method. *Comput. Electron. Agric.* **2021**, *180*, 105893. [CrossRef]
17. Zhang, S.; Jia, X.; Dong, J.; Wang, X.; Zhao, H.; Chen, X.; Zhang, Z.; Huang, Y.; Shi, J. Optimization of operating angles of disc coulters for maize residue management using discrete element method. *Comput. Electron. Agric.* **2024**, *218*, 108691. [CrossRef]
18. Zou, L.; Yan, D.; Niu, Z.; Yuan, J.; Cheng, H.; Zheng, H. Parametric analysis and numerical optimisation of spinach root vibration shovel cutting using discrete element method. *Comput. Electron. Agric.* **2023**, *212*, 108138. [CrossRef]
19. Zhao, S.; Wang, J.; Yang, C.; Chen, J.; Yang, Y. Design and Experiment of Stubble Chopper under Conservation Tillage. *Trans. Chin. Soc. Agric. Mach.* **2019**, *50*, 57–68.
20. Hu, M.; Gao, T.; Dong, X.; Tan, Q.; Yi, C.; Wu, F.; Bao, A. Simulation of soil-tool interaction using smoothed particle hydrodynamics (SPH). *Soil Tillage Res.* **2023**, *229*, 105671. [CrossRef]
21. Gao, T. The Study and Application of Soil-tool Interaction Numerical Model Based on SPH. Master's Thesis, Southwest University, Chongqing, China, 2023.
22. Zhong, J.; Jiang, J.; Jiang, T.; Zhao, Z.; Qiao, X.; Zhang, X. Deep-tillage Rotavator Technology Based on Smoothed Particle Hydrodynamics Simulation. *J. Mech. Eng.* **2010**, *46*, 63–69. [CrossRef]
23. Yang, W.; Zhang, X.; Yang, J.; Zheng, X.; Liao, L. Simulation and test on performance of soil-cassava jitter separation device of cassava harvester. *Trans. Chin. Soc. Agric. Eng.* **2017**, *33*, 18–25.
24. Kang, J.; Li, S.; Yang, X.; Liu, L.; Li, C. Experimental verification and simulation analysis on power consumption of disc type ditcher. *Trans. Chin. Soc. Agric. Eng.* **2016**, *32*, 8–15.

25. Lu, C.; He, J.; Li, H.; Wang, Q.; Zheng, Z.; Zhang, X. Simulation of Soil Cutting Process by Plane Blade Based on SPH Method. *Trans. Chin. Soc. Agric. Mach.* **2014**, *45*, 134–139.
26. He, X.; Xia, J.; Yu, S. Finite element simulation of soil cutting with rotary knife roller based on ANSYS/LS-DYNA. *Trans. Chin. Soc. Agric. Eng.* **2013**, *29*, 34–41+293.
27. Yang, W.; Yang, J.; Jia, F.; Wang, Q.; Huang, Y. Numerical Simulation of Digging Operation of Cassava Root Planted in Red Clay. *J. Mech. Eng.* **2013**, *49*, 135–143. [CrossRef]
28. Yang, W.; Tian, A.; Ye, R.; Liu, H.; Zhang, Z.; Wang, Q. Numerical simulation research on the penetration resistance of aluminum foam sandwich plate based on SPH-FEM coupling method. *Ship Sci. Technol.* **2023**, *45*, 13–19.
29. Zhang, Z.; Qiang, H.; Gao, W. Coupling of smoothed particle hydrodynamics and finite element method for impact dynamics simulation. *Eng. Struct.* **2010**, *33*, 255–264. [CrossRef]
30. Tagar, A.A.; Ji, C.; Adamowski, J.; Malard, J.; Chen, S.; Ding, Q.; Abbasi, N.A. Finite element simulation of soil failure patterns under soil bin and field testing conditions. *Soil Tillage Res.* **2015**, *145*, 157–170. [CrossRef]
31. Yang, W.; Mo, X.; Yang, J.; Yuan, F.; Huang, S. Experimental Study on the Basic Parameters of Sugarcane on Easy Lodging Period. *J. Agric. Mech. Res.* **2016**, *38*, 143–148.
32. Xiao, H.; Zhao, Y.; Ding, W.; Mei, S.; Han, Y.; Zhang, Y.; Yan, H.; Song, Z. Design and experiment on blade shaft of 1KS60-35X type orchard double-helix trenching and fertilization machine. *Trans. Chin. Soc. Agric. Eng.* **2017**, *33*, 32–39.
33. Yang, W.; Yang, J.; Liu, Z. Dynamic simulation experiment on effects of sugarcane cutting beneath surface soil. *Trans. Chin. Soc. Agric. Eng.* **2011**, *27*, 150–156.
34. Zhang, J.; Liu, H.; Gao, J.; Lin, Z.; Chen, Y. Simulation and Test of Corn Layer Alignment Position Hole Fertilization Seeder Based on SPH. *Trans. Chin. Soc. Agric. Mach.* **2018**, *49*, 66–72.
35. Wu, T.; Jiang, L.; Lai, Y.; Ma, X. Numerical Simulation of Roots-soil Separation Process of Corn Stubble. *J. Henan Agric. Sci.* **2016**, *45*, 132–136.